Available online at www.sciencedirect.com
SCIENCE DIRECT®
Materials Research Bulletin 40 (2005) 177–186
Materials Research Bulletin
www.elsevier.com/locate/matresbu

Cr^{3+} modified $LiMn_2O_4$ spinel intercalation cathodes through oxalic acid assisted sol–gel method for lithium rechargeable batteries

R. Thirunakaran[a,*], Ki-Tae Kim[b], Yong-Mook Kang[b], Jai Young-Lee[b]

[a]*Central Electrochemical Research Institute, Karaikudi 630006, India*
[b]*Department of Material Science and Engineering, Korea Advanced Institute of Science and Technology, 373-1, Gusong-Dong, Yusong-Gu, Daejon, Republic of South Korea*

Received 6 June 2003; received in revised form 18 May 2004; accepted 31 August 2004

Abstract

To improve the cycle performance of eco-friendly and cost-effective spinel $LiMn_2O_4$ as the cathode of 4 V class Li secondary batteries, the spinel phase $LiCr_xMn_{2-x}O_4$ ($x = 0.01$–0.20) was synthesized by soft chemistry method using oxalic acid as chelating agent. The present technique results in better homogeneity, good surface morphology, shorter heat treatment time, sub-micron sized particles, good agglomeration and better crystallinity. Electrochemical studies were monitored in the potential range of 3–4.5 V. The present paper reveals that chromium substituted manganese spinel improves the structural stability of the parent material.

Keywords: B. Intercalation reaction; D. Electrochemical properties; B. Sol–gel chemistry; C. X-ray diffraction; D. Energy storage

1. Introduction

The $LiMn_2O_4$ spinel is preferred as one of the most promising cathode material for rechargeable lithium batteries because of its low cost and environmentally benign nature. Although $LiMn_2O_4$ cycles well at room temperature, prolonged cycling at higher temperatures is accompanied by an unacceptable

* Corresponding author. Tel.: +91 456522322; fax: +91 456537779.
E-mail address: rthirunakaran@yahoo.com (R. Thirunakaran).

0025-5408/$ – see front matter
doi:10.1016/j.materresbull.2004.08.013

capacity fade [1,2]. This capacity fade has been attributed due to several factors such as electrolyte decomposition, slow dissolution of $LiMn_2O_4$ [3] unstable two phase reaction, Jahn–Teller distortion [4], lattice instability [5] and particle disruption [6]. Ohzuku et al. [7] studied a series of 5 V cathode materials obtained by substituting Mn in $LiMn_2O_4$ with 3d transition metals such as Co, Cr, Cu, Fe, Ni, Ti and Zn, which are shown to be effective in surpassing the capacity fade upon cycling. These materials showed operating voltages above 4.8 V as reported by Lee et al. [8] also. In this regard, Cr as a dopant in $LiMn_2O_4$ is also expected to exhibit an excellent electrochemical reversibility upon cycling. In other words, reduced particle size that enhances the cycleability and rate capability of the positive electrode has also been aimed at in the present investigation. It is well known that the physical as well as the electrochemical properties of any cathodes depends upon the method of synthesis and the types of precursors employed. In recent years, several low-temperature preparation methods have been used such as sol–gel [9,10], precipitation [11], Pechini process [12] and the hydrothermal method [13]. In this work, we have made an attempt to stabilize the $LiMn_2O_4$ spinel structure by sol–gel method, using oxalic acid as a chelating agent with Cr as a dopant, which has not been previously reported. It is noteworthy to mention that the soft chemistry techniques have many advantages such as better homogeneity, low calcinations temperature, shorter heating time, regular morphology, sub-mircon sized particles, less impurities, large surface area and good control of stoichiometry. Therefore, the same has been chosen to be employed for the present study to synthesize a series of Cr-doped $LiMn_2O_4$ solid solutions.

2. Experimental

$LiCr_xMn_{2-x}O_4$ ($x = 0.01$, 0.02, 0.05, 0.10, 0.20) powders have been synthesized by the sol–gel method using oxalic acid as chelating agent (Plate 1). Stoichiometric amounts of lithium nitrate, manganese nitrate and ammonium dichromate, were thoroughly mixed and dissolved in deionized water. The solution was stirred continuously along with mild heating to ensure homogeneity and a solution of oxalic acid was added to the homogenous solution. The addition of oxalic acid resulted in the formation of a precipitate, the intensity of which increased with the addition of an increasing amount of oxalic acid. Simultaneously, pH of the solution was adjusted between 7 and 8.5. The process of stirring and heating was continued until a solidified mass was obtained. The gel, thus obtained, was heated initially in a heating oven at 110 °C overnight and then further, in a heating furnace at 400 °C for about 4 h. The powder obtained was further heated to 800 °C for 4 h to ensure better purity and crystallinity. Ultimately, the fine powders resulting from the above processes have been collected and subjected to physical as well as electrochemical characterizations.

2.1. Electrode preparation

Standard 2016 coin cells were assembled using lithium metal as an anode, a Celgard 2400 separator and 1 M solution of $LiPF_6$ in a 50:50 (v/v) mixture of ethylene carbonate and dimethyl carbonate. Cathodes were 1.8 cm diameter aluminum disc spread-coated with a 80:10:10 slurry of the cathode active powder, graphite and poly-vinylidene fluoride in *N*-methyl-2-pyrrolidone. Cathode active material loadings in the samples varied from 0.087 to 0.098 g. Charge–discharge studies were performed using an in-house charging facility between 3 and 4.4 V.

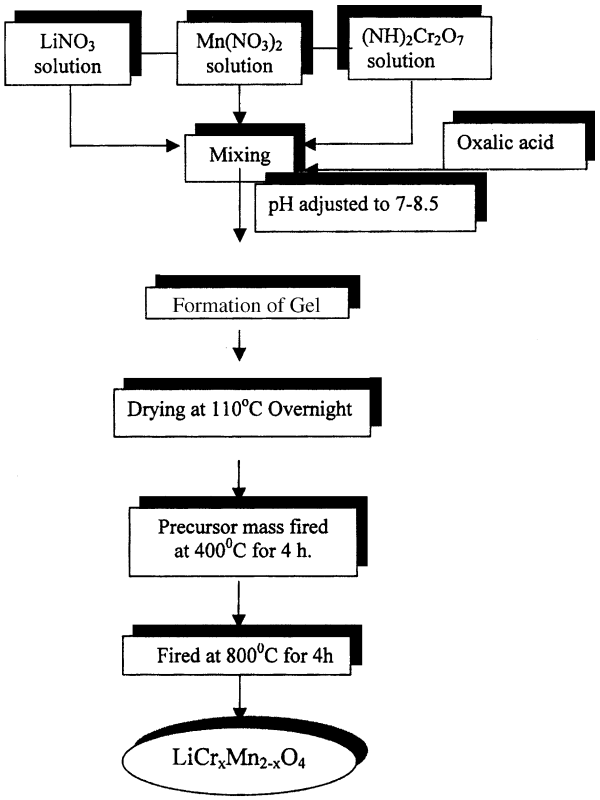

Plate 1. Flow chart for the synthesis of $LiCr_xMn_{2-x}O_4$ via oxalic acid assisted sol–gel route.

X-ray diffraction studies were made on a Jeol JDX 8030 X-ray diffractometer (XRD) with nickel-filtered Cu Kα radiation, in order to study the crystalline phase of the synthesized spinel. Surface morphology was examined using JEOL JSM 1200 EX II, The Netherlands. Charge–discharge studies were carried out using TOSCAT-3000V, battery-testing unit, Japan. The cells were assembled in an argon-filled glove box (Mbraun) with moisture and oxygen levels maintained at less than 1 ppm. Charge–discharge studies were completed at room temperature using WONATECH (South Korea) company battery tester.

3. Results and discussion

3.1. X-ray diffraction studies

The X-ray diffraction patterns of Cr^{3+}-doped samples show a striking similarity to that of pure $LiMn_2O_4$ (space group Fd3m) in which the manganese ions occupy the 16d sites and the O^{2-} ions occupy the 32e sites (Fig. 1). The fact that chromium-doped compounds have a cubic spinel structure has been demonstrated by several people [14–16]. In fact, the lattice parameter of $LiCr_xMn_{2-x}O_4$ is very close to that of $LiMn_2O_4$ [17–19]. Substitution of manganese with chromium should result in a shrinkage of the

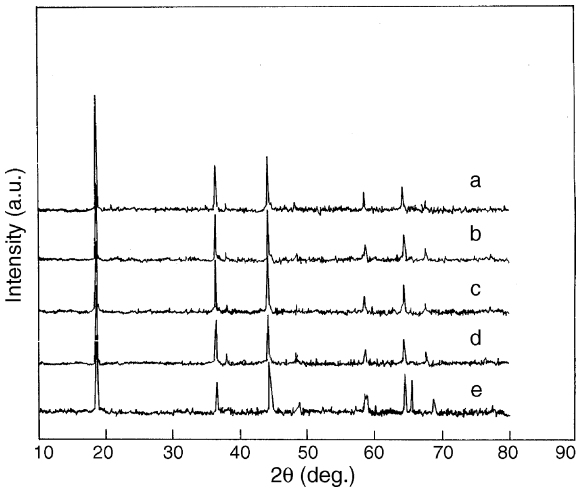

Fig. 1. XRD pattern of $LiMn_2O_4$ and $LiCr_xMn_{2-x}O_4$ samples calcined at 800 °C for 8 h: (a) 0.00, (b) $x = 0.01$, (c) $x = 0.02$, (d) $x = 0.05$, (e) $x = 0.10$, (f) $x = 0.20$.

unit cell volume. This is because in the same oxidation state chromium ions have smaller ionic radii than manganese ions; Cr^{3+} (0.615 Å) Mn^{3+} (0.68 Å), Cr^{4+} (0.58 Å), Mn^{4+} (0.60 Å) [20]. The decrease in cell volume should increase the stability of the structure during deintercalation and intercalation of lithium [21–23]. The stronger Cr–O bonds in the delithated state (compare the binding energy 1142 kJ/mole for CrO_2 with 946 kJ/mole for α-MnO_2) may also be expected to contribute to the stabilization of the octahedral sites. The higher stabilization energy of Cr^{3+} ions for octahedral coordination is well known. Lately, Sigala et al. [21] demonstrated the structural stability imparted by Cr^{3+} ions to $LiMn_2O_4$ spinels, while [22] demonstrated a similar effect by a chemically modified Cr^{5+} to Cr^{6+} oxide. The incorporation of Cr^{3+} greatly suppresses the dissolution of manganese ions in the electrolyte (one of the failure mechanisms of the $LiMn_2O_4$ cathode) has been shown by Iwata et al. [23]. The lattice parameters of $LiMn_2O_4$ and $LiCr_xMn_{2-x}O_4$ are shown in Table 1. The lattice parameters began to diminish starting when mCrO was doped into the spinel under pressure. The calculated lattice values for $y = 0.00$, 0.02, 0.05 and 0.10 in $LiCr_xMn_{2-x}O_4$ were 8.220, 8.218, 8.220 and 8.214 Å.

3.2. Surface morphology

Fig. 2(a–f) depicts the transmission electron micrographs (TEM) of pure and Cr-doped samples of $LiMn_2O_4$. As observed from figures, the particles become agglomerated with an increase in chromium

Table 1
Unit cell parameters and inter atomic distance for $LiCr_xMn_{2-x}O_4$ from ammonium dichromate precursor

$LiCr_xMn_{2-x}O_4$	a (Å)	V (Å)	$R_{Mn–Mn(Cr)}$ (Å)	$R_{Mn(Cr–O)}$ (Å)
$LiMn_2O_4$ ($y = 0.00$)	8.220	555.5 (2)	2.908	1.950
$LiCr_{0.02}Mn_{1.95}O_2$ ($y = 0.02$)	8.218 (1)	553.2 (2)	2.904	1.940
$LiCr_{0.05}Mn_{1.95}O_2$ ($y = 0.05$)	8.220 (1)	554.2 (2)	2.906	1.938
$LiCr_{0.01}Mn_{1.90}O_2$ ($y = 0.10$)	8.214 (1)	552.5 (2)	2.905	1.936

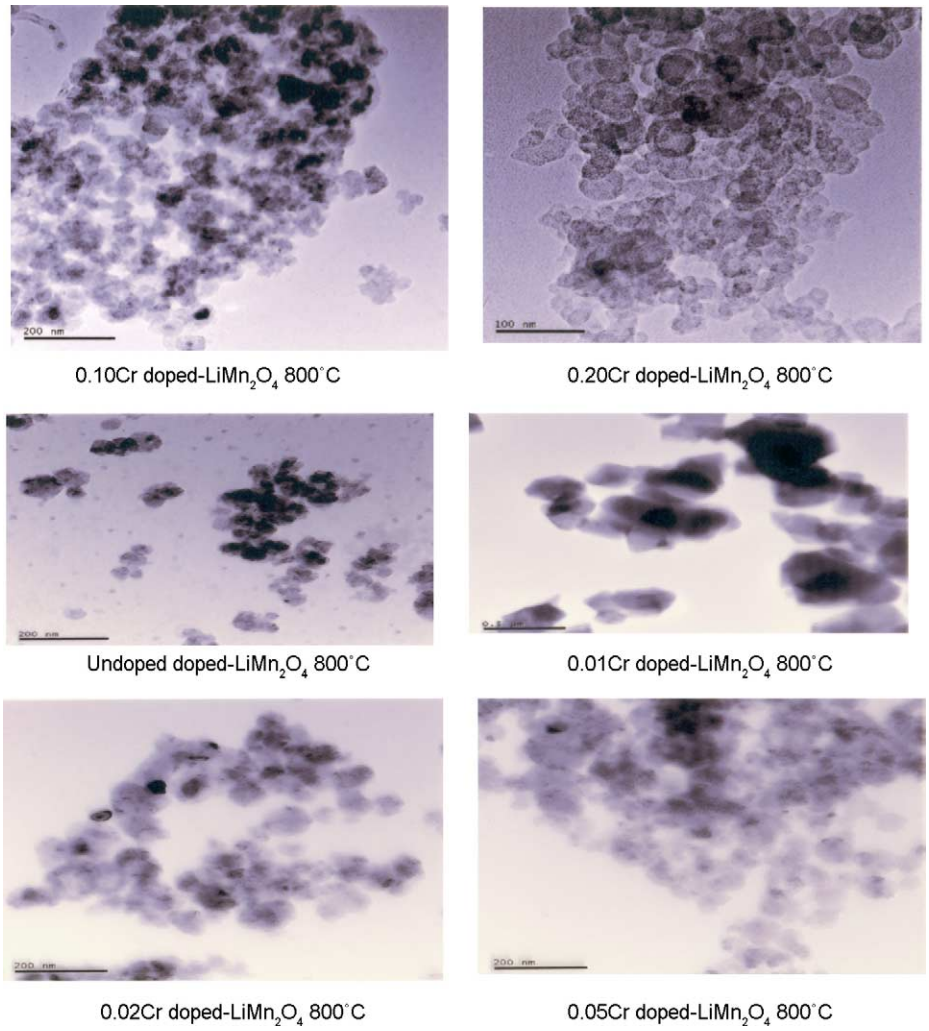

Fig. 2. Transmission electron micrographs of $LiMn_2O_4$ and $LiCr_xMn_{2-x}O_4$ samples calcined at 800 °C for 8 h: (a) 0.00, (b) $x = 0.01$, (c) $x = 0.02$, (d) $x = 0.05$, (e) $x = 0.10$, (f) $x = 0.20$.

content. Furthermore, the increase in agglomeration of the particles results in effective inter-particle contact leading to good capacity, and good cycleability. However, it is interesting to note that the composition with lower Cr doping results in a slightly higher capacity than the undoped $LiMn_2O_4$. Moreover, at the higher doping (Fig. 2d–f) the decrease of capacity due to the decrease of manganese ions results, eventhough particles are well agglomerated.

3.3. EDAX studies

Fig. 3(a–f) represents the atomic percentage compositions of Cr and Mn in the synthesized $LiMn_2O_4$ and $LiCr_xMn_{2-x}O_4$ compounds. It is observed that the peak located around 5.5 keV starts going with

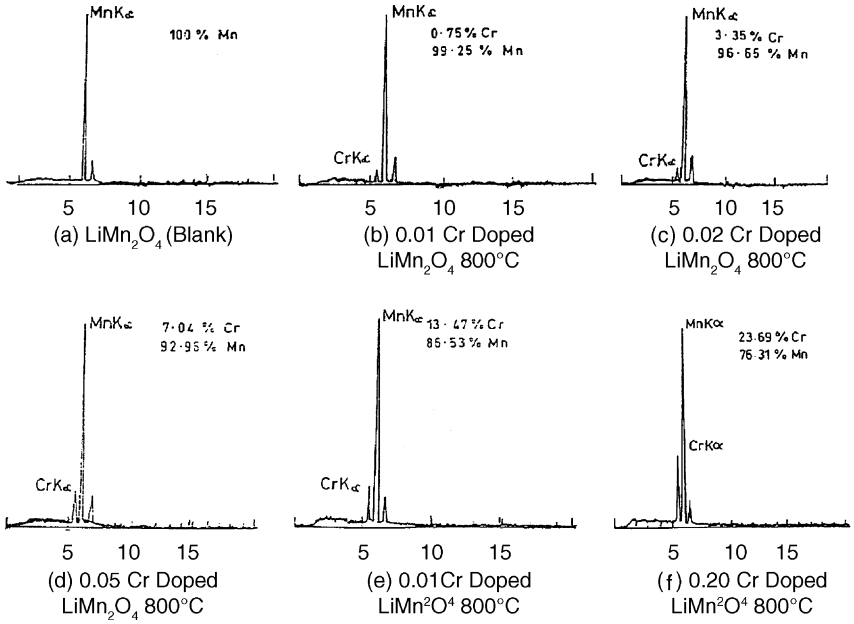

Fig. 3. Atomic percentage compositions of $LiMn_2O_4$ and $LiCr_xMn_{2-x}O_4$ samples calcined at 800 °C for 8 h: (a) 0.00, (b) $x = 0.01$, (c) $x = 0.02$, (d) $x = 0.05$, (e) $x = 0.10$, (f) $x = 0.20$.

increase in Cr content of the synthesized material. Further, as seen from Fig. 3(a) this peak is absent thereby confirming the presence of dopant Cr stoichiometry in the materials (Fig. 3b–f). Table 2 shows the EDAX results of the atomic percentage compositions of Cr and Mn in the synthesized $LiMn_2O_4$ and $LiCr_xMn_{2-x}O_4$ compounds.

3.4. Charge–discharge studies

Fig. 4 depicts the charge–discharge curves of $LiMn_2O_4$ and $LiCr_xMn_{2-x}O_4$ compounds. These cells were cycled between 3 and 4.25 at 0.1 and 0.2 C rate and the initial specific capacities delivered are 130 and 120 mAh/g. Capacities above 4.25 V were not tapped for fear of electrolyte decomposition at such voltages. The capacities obtained correspond to the oxidation of Mn^{3+} to Mn^{4+} and Cr^{3+}/Cr^{4+}.

Table 2
Shows the EDAX results of the atomic percentage compositions of Cr and Mn in the synthesized $LiMn_2O_4$ and $LiCr_xMn_{2-x}O_4$ compounds

Sample numbers	Atomic percentage composition of Cr (%)	Atomic percentage composition of Mn (%)
(a)	–	100
(b)	0.75	99.25
(c)	3.35	96.25
(d)	7.04	92.96
(e)	13.47	86.53
(f)	23.69	76.31

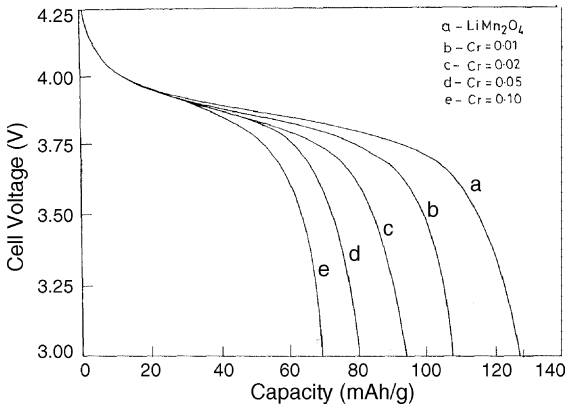

Fig. 4. Charge–discharge behavior of $LiMn_2O_4$ and $LiCr_xMn_{2-x}O_4$ cells: (a) 0.00, (b) $x = 0.01$, (c) $x = 0.02$, (d) $x = 0.05$, (e) $x = 0.10$.

The oxidation of Cr^{3+} to Cr^{4+} occurs at 4.8 V [24–26]. The two-step deintercalation/intercalation process in the case of chromium-doped $LiMn_2O_4$ may for example be represented as follows:

$$Li[Cr^{3+}yMn^{3+}Mn^{4+}]O_4 \overset{4\,V}{\longleftrightarrow} 1 - yLi_y[Cr^{3+}Mn^{4+}]O_4 + (1-y)Li^+ + (1-y)$$
$$e^- \overset{4.8\,V}{\longleftrightarrow} Cr^{4+}yMn^{4+}]O_4 + yLi^+ + ye^-$$

While in the case of Cr^{3+} doped $LiMn_2O_4$ the Cr^{3+} ions would replace the Mn^{3+} ions, reducing the 4 V capacity of the compound. During the first cycles, the $LiMn_2O_4$ spinel exhibits the specific capacity of 128 mAh/g, whereas 0.01 Cr-doped spinel is bestowed with slightly lower capacity than pure $LiMn_2O_4$. Replacement of Mn^{3+} ion by Cr^{3+} and the oxidation of a similar amount of Mn^{3+} to the Mn^{4+} state, leads to an increase in the average oxidation state of manganese. The diminished Mn^{3+} ion concentration can contribute to a reduced unit cell volume of the spinel, which results in an increased structural stability. The capacities obtained correspond to the oxidation of Mn^{3+} to Mn^{4+}. Similarly, the oxidation of Cr^{3+} to Cr^{4+} occurs at 4.8 V [27].

3.5. Cycleability studies

The typical graph in Fig. 5 shows that the pure $LiMn_2O_4$ and chromium-doped spinel and the 0.01 chromium-doped $LiMn_2O_4$ exhibit constant capacity of 110 mAh/g up to 100 cycles. Despite the fact that the pristine $LiMn_2O_4$ exhibits initially higher capacity 118 mAh/g than 0.01 Cr-doped $LiMn_2O_4$ (110 mAh/g), its capacity has been decreased drastically. The better cycleability of the doped variety is due to the increased stability caused by higher octahedral site stabilization energy of Cr^{3+}. Thus, the effect of chromium is more pronounced in reducing the capacity fade. Furthermore, the ionic radius of Cr^{3+} is lower than Mn^{3+}, i.e. 0.615 Å, whereas Mn^{3+}, Cr^{4+} and Mn^{4+} have a radius of 0.68, 0.58 and 0.60 Å, respectively. Hence, the decrease in cell volume increases the stability of the structure during deintercalation/intercalation of lithium. Thus, the Cr dopant stabilizes the Mn^{3+} structure for increasing good cycleability.

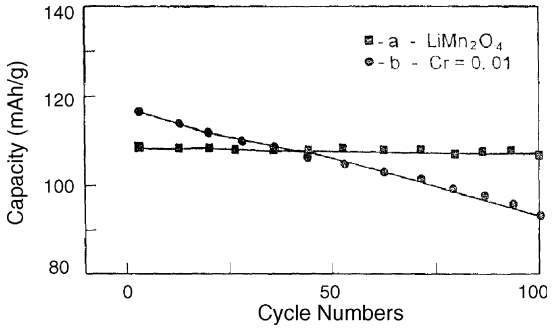

Fig. 5. Cycling performance of $LiMn_2O_4$ and $LiCr_{0.01}Mn_{1.99}O_4$ cells: (a) 0.00, (b) $x = 0.01$, (c) $x = 0.02$, (d) $x = 0.05$, (e) $x = 0.10$, (f) $x = 0.20$.

3.6. Cyclic voltammogram

Fig. 6(a and b) depicts the cyclic voltammogram (sweep rate: 0.02 mV/s) of the cells employing $LiMn_2O_4$ and $LiCr_{0.01}Mn_{1.9}O_4$, respectively. Despite electrolyte decomposition occurring at such a high voltage, there was no evidence of such a process in the voltammograms. In fact, $LiPF_6$-based electrolytes, such as the one used in this study, are fairy tolerant to high voltages [28]. Furthermore, the difference in capacities observed in Figs. 5 and 6, respectively, is due to the experimental conditions employed viz., in CV studies the experiments were carried out in a three electrode glass cell, whereas in the case of the cycling studies: two electrode coin cells were used. Generally, the anodic and cathodic peak appearing on the cyclic voltammogram are related to the insertion and extraction of lithium ions in the spinel. In the pristine $LiMn_2O_4$, the peak around 4.08 V corresponding to the lithium deintercalation/intercalation into/from the 8a tetrahedral sites, associated with the Mn^{4+}/Mn^{3+} couple and other peak in the $LiCr_{0.01}Mn_{1.99}O_4$ around 4.22 V, corresponds to the oxidation/reduction of the Cr^{3+}/Cr^{4+} couple [29,30]. The cyclic voltammogram for the chromium-doped spinel reveals that there is an increase in both the anodic and cathodic peak current and a decrease in peak separation when compared to the undoped spinel. This observation suggests that the chromium-doped spinel inherits an enhanced reversibility as well as rate capability.

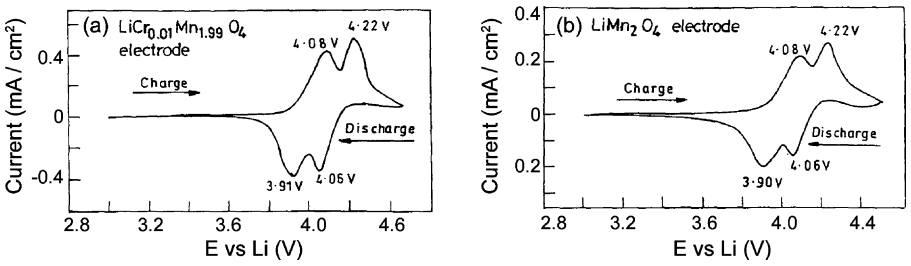

Fig. 6. Cyclic voltammogram of (a) $LiMn_2O_4$ and (b) $LiCr_{0.01}Mn_{1.99}O_4$ vs. at sweep rate 0.02 mV/s.

4. Conclusion

A new route for the synthesis of $LiMn_2O_4$ and $LiCr_xMn_{2-x}O_4$ has been adopted via an oxalic acid assisted sol–gel method. The sol–gel method rendered advantages such as a pure spinel phase, lower calcination temperature, and relatively shorter processing time with sub-micron sized particles and narrow particle size distribution, as expected.

XRD and TEM studies are in favor of the phase purity and well-defined particles of better morphology, respectively. Charge–discharge studies established the possibility of producing enhanced structural stability of the $LiCr_xMn_{2-x}O_4$ spinels through the Cr dopant. Cyclic voltammetry experiments show enhanced reversibility and rate capability of a Cr^{3+} modified spinel compared to the undoped spinel. It is further understood, from the present investigation, that the oxalic acid assisted sol–gel method of synthesis of $LiCr_xMn_{2-x}O_4$ ($x = 0.001$, 0.02, 0.05, 0.10, 0.20) has resulted in the formation of structurally stabilized spinel for better electrochemical behavior.

Acknowledgements

Dr. R. Thirunakaran would like to thank Professor Jai Young-Lee, for having arranged a Post Doctoral Fellowship for one year through Brain Korea 21, Republic of South Korea and for carrying out this work at the Korea Advanced Institute of Science and Technology (KAIST).

References

[1] Y. Xia, M. Yoshio, J. Electrochem. Soc. 144 (1977) 2593.
[2] G. Pistoia, A. Antonini, R. Rosati, D. Zane, Electrochim. Acta 41 (1996) 2863.
[3] D.H. Jang, J.Y. Shin, S.M. Oh, J. Electrochem. Soc. 143 (1996) 2204.
[4] R.J. Gummow, A. Dckock, M.M. Thackeray, Solid State Ionics 69 (1994) 59.
[5] A. Yamada, J. Solid State Chem. 122 (1996) 100.
[6] S.T. Myung, H.T. Chung, S. Komaba, N. Kumagai, H.B. Gu, J. Power Sources 90 (2000) 103.
[7] T. Ohzuku, S. Takeda, M. Iwanaga, J. Power Sources 81/82 (1999) 90.
[8] J.H. Lee, J.K. Hong, D.H. Jang, Y.K. Sun, S.M. Oh, J. Power Sources 89 (2000) 7.
[9] S. Bach, M. henry, N. Baffier, J.J. Livage, Solid State Chem. 80 (1990) 325.
[10] J.P. Pereira-Romas, J. Power Sources 54 (1995) 120.
[11] P. Barboux, J.M. Tarascon, F.K. Shokoohi, J. Solid State Chem. 94 (1991) 185.
[12] W. Liu, Gc. Farrington, F. Chaput, B.J. Dunn, J. Electrochem. Soc. 143 (1993) 879.
[13] M.S. Whittingam, Solid State Ionics 86 (1996) 88.
[14] G. Pistoia, G. Wang, C. Wang, Solid State Ionics 58 (1992) 285.
[15] W. Baochen, X. Yongyao, F. Li, Z. Dongjinang, J. Power Sources 43/44 (1993) 539.
[16] L. Guohua, H. Dcuta, T. Uchida, M. Wakihara, J. Electrochem. Soc. 143 (1996).
[17] A. Mosbach, A. Verbaere, M. Tournoux, Mater. Res. Bull. 18 (1983) 1375.
[18] M.M. Thackeray, WI.F. David, P.G. Bruce, J.B. Goodenough, Mater. Res. Bull. 19 (1983) 99.
[19] WIF. David, M.M. Thackeray, P.G. Bruce, J.B. Goodenough, Mater. Res. Bull. 19 (1984) 99.
[20] W. Borchardt-Ott, Crystallography, Springer, New York, 1993.
[21] C. Sigala, D. Guyomard, A. Verbaere, Y. Piffard, M. Tournoux, Solid State Ionics 81 (1995) 167.
[22] D. Zhang, B.N. Popov, R.E. White, J. Power Sources 76 (1998).
[23] E. Iwata, K. Takahashi, T. Maeda, T. Mouri, J. Power Sources 81/82 (1999) 430.

[24] C. Sigala, D. Guyomard, A. Verbaere, Y. Piffard, M. Tournoux, Solid State Ionics 81 (1995) 167.
[25] C. Sigala, M. Tournoux, J. Solid State Chem. 132 (1997) 372.
[26] H. Kawai, M. Nagata, H. Tukamotao, A.R. West, J. Power Sources 81/82 (1999) 67.
[27] X. Yia, M. Yoshio, J. Electrochem. Soc. 143 (1996) 825.
[28] C. Sigala, A. Le Gal La Salle, Y. Piffard, D. Guyomard, J. Electrochem. Soc. 148 (2001) A812.
[29] C. Sigala, D. Guyomard, A. Verbaere, Y. Piffard, M. Tournoux, Solid State Ionics 81 (1995) 167.
[30] H. Kawai, M. Nagata, H. Tukamoto, A.R. West, J. Power Sources 81/82 (1999) 67.